Hybrid interconnection of iterative bidding and power network dynamics for frequency regulation and optimal dispatch

Tjerk Stegink, Ashish Cherukuri, Claudio De Persis, Arjan van der Schaft, and Jorge Cortés

***Abstract*—This paper considers a real-time electricity market involving an independent system operator (ISO) and a group of strategic generators. The ISO operates a market where generators bid prices at which there are willing to provide power. The ISO makes power generation assignments with the goal of solving the economic dispatch problem and regulating the network frequency. We propose a multi-rate hybrid algorithm for bidding and market clearing that combines the discrete nature of iterative bidding with the continuous nature of the frequency evolution in the power network. We establish sufficient upper bounds on the inter-event times that guarantee that the proposed algorithm asymptotically converges to an equilibrium corresponding to an efficient Nash equilibrium and zero frequency deviation. Our technical analysis builds on the characterization of the robustness properties of the continuous-time version of the bidding update process interconnected with the power network dynamics via the identification of a novel LISS-Lyapunov function. Simulations on the IEEE 14-bus system illustrate our results.**

I. Introduction

The dispatch of power generation in the grid has been traditionally done in a hierarchical fashion. Broadly speaking, cost efficiency is ensured via market clearing at the upper layers and frequency regulation is achieved via primary and secondary controllers at the bottom layers. Research on improving the performance of these layers has mostly developed independently from each other, motivated by their separation in time-scales. The increasing penetration of renewables poses significant challenges to this model of operation because of its intermittent and uncertain nature. At the same time, the penetration of renewables also presents an opportunity to rethink the architecture and its hierarchical separation towards the goal of improving efficiency and adaptivity. A key aspect to achieve the integration of different layers is the characterization of the robustness properties of the mechanisms used at each layer, since variables at the upper layers cannot be assumed in steady state any more at the lower ones. These considerations motivate our work on iterative bidding schemes combined with continuous physical network dynamics and the correctness analysis of the resulting multi-rate hybrid interconnected system.

A preliminary version of this work appeared as [1] at the American Control Conference.

This work is supported by the NWO *Uncertainty Reduction in Smart Energy Systems (URSES)* program and the ARPA-e *Network Optimized Distributed Energy Systems (NODES)* program.

T. W. Stegink, C. De Persis and A. J. van der Schaft are with the Jan C. Willems Center for Systems and Control, University of Groningen, 9747 AG Groningen, the Netherlands. {t.w.stegink, c.de.persis, a.j.van.der.schaft}@rug.nl

A. Cherukuri is with the Automatic Control Laboratory, ETH Zürich. cashish@control.ee.ethz.ch

J. Cortés is with the Department of Mechanical and Aerospace Engineering, University of California, San Diego. cortes@ucsd.edu

Literature review: The integration of economic dispatch and frequency regulation in power networks has attracted increasing attention in the last decades. Many recent works [2], [3], [4], [5], [6], [7], [8] envision merging the design of primary, secondary, and tertiary control layers for several models of the power network/micro-grid dynamics with the aim of bridging the gap between long-term optimization and real-time frequency control. In scenarios where generators are price-takers, the literature has also explored the use of market mechanisms to determine the optimal allocation of power generation and to stabilize the frequency with real-time (locational marginal) pricing, see [9], [10], [11], [12]. Inspired by the iterative bidding schemes for strategic generators proposed in [13], that lead to efficient Nash equilibria where power generation levels minimize the total cost as intended by the ISO, our work [14] has shown that the integration with the frequency dynamics of the network can also be achieved in scenarios where generators are price-bidders. However, this integration relies on a continuous-time model for the bidding process, where the frequency coming from the power network dynamics enters as a feedback signal in the negotiation process. Instead, we account here for the necessarily discrete nature of the bidding process and explore the design of provably correct multi-rate hybrid implementations that realize this integration.

Statement of contributions: We consider an electrical power network consisting of an ISO and a group of strategic generators. The ISO seeks to ensure that the generation meets the load with the minimum operation cost and the grid frequency is regulated to its nominal value. Each generator seeks to maximize its individual profit and does not share its cost function with anyone. The ISO operates the market, where generators bid prices at which there are willing to provide power, and makes power generation assignments based on the bids and the local frequency measurements. Our goal is to design mechanisms that ensure the stability of the interconnection between the ISO-generator bidding process and the physical network dynamics while accounting for the different nature (iterative in the first case, evolving in continuous time in the second) of each process. Our starting point is a continuous-time bid update scheme coupled with the physical dynamics of the power network whose equilibrium corresponds to an efficient Nash equilibrium and zero frequency deviation. Our first contribution is the characterization of the robustness properties of this dynamics against additive disturbances. To achieve this, we identify a novel local Lyapunov function that includes the energy function of the closed-loop system. The availability of this function not only leads us to establish local exponential convergence to the desired equilibrium, but also allows us rigorously establish its local input-to-state stability properties.

Building on these results, our second contribution develops a time-triggered hybrid implementation that combines the discrete nature of iterative bidding with the continuous nature of the frequency evolution in the power network. In our design, we introduce two iteration loops, one (faster) inner-loop for the bidding process that incorporates at each step the frequency measurements, and one (slower) outer-loop for the market clearing and the updates in the power generation levels, that are sent to the continuous-time power network dynamics. We refer to this multi-rate hybrid implementation as time-triggered because we do not necessarily prescribe the time schedules to be periodic. To analyze its convergence properties, we regard the time-triggered implementation as an approximation of the continuous-time dynamics and invoke the robustness properties of the latter, interpreting as a disturbance their mismatch. This allows us to derive explicit upper bounds on the length between consecutive triggering times that guarantee that the time-triggered implementation remains asymptotically convergent. The computation of these upper bounds does not require knowledge of the efficient Nash equilibrium. Simulations on the IEEE 14-bus power network illustrate our results.

Outline: The paper is organized as follows. Section II introduces the dynamic model of the power network and Section III describes the problem setup. Section IV characterizes the robustness properties of the continuous-time dynamics resulting from the interconnection of bid updating and network dynamics. Section V introduces the time-triggered implementation and identifies sufficient conditions on the inter-event times that ensure asymptotic convergence to efficient Nash equilibria. Simulations illustrate the results in Section VI. Section VII gathers our conclusions and ideas for future work. The appendices contain the proofs of the main results of the paper.

Notation: Let $\mathbb{R}, \mathbb{R}_{\geq 0}, \mathbb{R}_{>0}, \mathbb{Z}_{\geq 0}, \mathbb{Z}_{\geq 1}$ be the set of real, nonnegative real, positive real, nonnegative integer, and positive integer numbers, respectively. For $m \in \mathbb{Z}_{\geq 1}$, we use the shorthand notation $[m] = \{1, \dots, m\}$. For $A \in \mathbb{R}^{m \times n}$, we let $\|A\|$ denote the induced 2-norm. Given $v \in \mathbb{R}^n, A = A^T \in \mathbb{R}^{n \times n}$, we denote $\|v\|_A^2 := v^T A v$. The notation $\mathbb{1} \in \mathbb{R}^n$ is used for the vector whose elements are equal to 1. The Hessian of a twice-differentiable function $f : \mathbb{R}^n \to \mathbb{R}$ is denoted by $\nabla^2 f$.

II. Power network frequency dynamics

Here we present the model of the physical power network that describes the evolution of the grid frequency. The network is represented by a connected, undirected graph $\mathcal{G} = (\mathcal{V}, \mathcal{E})$, where nodes $\mathcal{V} = [n]$ represent buses and edges $\mathcal{E} \subset \mathcal{V} \times \mathcal{V}$ are the transmission lines connecting the buses. Let m denote the number of edges, arbitrarily labeled with a unique identifier in $[m]$. The ends of each edge are also arbitrary labeled with '+' and '-', so that we can associate to the graph the incidence matrix $D \in \mathbb{R}^{n \times m}$ given by

$$D_{ik} = \begin{cases} +1 & \text{if } i \text{ is the positive end of edge } k, \\ -1 & \text{if } i \text{ is the negative end of edge } k, \\ 0 & \text{otherwise.} \end{cases}$$

Each bus represents a control area and is assumed to have one generator and one load. Following [15], the dynamics at the buses is described by the *swing equations* (1).

$$\begin{aligned} \dot{\delta} &= \omega \\ M\dot{\omega} &= -D\Gamma \sin(D^T \delta) - A\omega + P_g - P_d \end{aligned} \tag{1}$$

Here $\Gamma = \operatorname{diag}\{\gamma_1, \dots, \gamma_m\} \in \mathbb{R}^{m \times m}, \gamma_k = B_{ij} V_i V_j$, where $k \in [m]$ corresponds to the edge between nodes i and j. Table I specifies the meaning of the symbols used in the model (1).

$\delta \in \mathbb{R}^n$	(vector of) voltage phase angles
$\omega \in \mathbb{R}^n$	frequency deviation w.r.t. the nominal frequency
$V_i \in \mathbb{R}_{>0}$	voltage magnitude at bus i
$P_d \in \mathbb{R}^n$	power load
$P_g \in \mathbb{R}^n$	power generation
$M \in \mathbb{R}_{\geq 0}^{n \times n}$	diagonal matrix of moments of inertia
$A \in \mathbb{R}_{\geq 0}^{n \times n}$	diagonal matrix of asynchronous damping constants
$B_{ij} \in \mathbb{R}_{\geq 0}$	negative of the susceptance of transmission line (i, j)

Table I: Parameters and state variables of model (1).

To avoid issues in the stability analysis of (1) due to the rotational invariance of δ, see e.g., [16], we introduce the new variable $\varphi = D_t^T \delta \in \mathbb{R}^{n-1}$. Here φ represents the voltage phase angle differences along the edges of a spanning tree of the graph $\mathcal{G}$ with incidence matrix D_t. The physical energy stored in the transmission lines is given by (2), where $D_t^\dagger = (D_t^T D_t)^{-1} D_t^T$ denotes the Moore-Penrose inverse of D_t.

$$U(\varphi) = -\mathbb{1}^T \Gamma \cos(D^T D_t^{\dagger T} \varphi). \tag{2}$$

By noting that $D_t D_t^\dagger D = (I - \frac{1}{n} \mathbb{1}\mathbb{1}^T) D = D$, the physical system (1) in the (φ, ω)-coordinates takes the form

$$\begin{aligned} \dot{\varphi} &= D_t^T \omega \\ M\dot{\omega} &= -D_t \nabla U(\varphi) - A\omega + P_g - P_d \end{aligned} \tag{3}$$

In the sequel we assume that, for the power generation $P_g = \bar{P}_g$, there exists an equilibrium $\operatorname{col}(\bar{\varphi}, \bar{\omega})$ of (3) that satisfies $D^T D_t^{\dagger T} \bar{\varphi} \in (-\frac{\pi}{2}, \frac{\pi}{2})^m$. The latter assumption is standard and often referred to as the *security constraint* [15].

III. Problem statement

In this section we formulate the problem statement and then discuss the paper objectives. We start from the power network model introduced in Section II and then explain the game-theoretic model describing the interaction between the ISO and the generators following the exposition of [17], [13].

The cost incurred by generator $i \in [n]$ in producing P_{gi} units of power is given by

$$C_i(P_{gi}) := \frac{1}{2} q_i P_{gi}^2 + c_i P_{gi}, \tag{4}$$

where $q_i > 0$ and $c_i \geq 0$. The total network cost is then

$$C(P_g) := \sum_{i \in [n]} C_i(P_{gi}) = \frac{1}{2} P_g^T Q P_g + c^T P_g, \tag{5}$$

with $Q = \mathrm{diag}\{q_1, \dots, q_n\}$ and $c = \mathrm{col}(c_1, \dots, c_n)$. Given the cost (5) and the power loads P_d, the ISO seeks to solve the *economic dispatch problem*

$$\underset{P_g}{\text{minimize}} \quad C(P_g), \tag{6a}$$

$$\text{subject to} \quad \mathbb{1}^T P_g = \mathbb{1}^T P_d, \tag{6b}$$

and, at the same time, regulate the network frequency to its nominal value. Since the function C is strongly convex, there exists a unique optimizer P_g^* of (6). However, we assume that the generators are strategic and they do not reveal their cost functions to anyone, including the ISO. Consequently, the ISO is unable to determine the optimizer of (6). Instead, it determines the power dispatch according to a market clearing procedure in which each generator submits bids to the ISO.

We consider price-based bidding: each generator $i \in [n]$ submits the price per unit electricity $b_i \in \mathbb{R}$ at which it is willing to provide power. Based on these bids, the ISO finds the power generation allocation that minimizes the total generator payment while meeting the load. More precisely, given the bid $b = \mathrm{col}(b_1, \dots, b_n)$, the ISO solves

$$\underset{P_g}{\text{minimize}} \quad b^T P_g, \tag{7a}$$

$$\text{subject to} \quad \mathbb{1}^T P_g = \mathbb{1}^T P_d. \tag{7b}$$

The optimization problem (7) is linear and may in general have multiple (unbounded) solutions. Among these solutions, let $P_g^{\text{opt}}(b) = \mathrm{col}(P_{g1}^{\text{opt}}(b), \dots, P_{gn}^{\text{opt}}(b))$ be the optimizer of (7) the ISO selects given bids b. Knowing this process, each generator i aims to bid a quantity b_i to maximize its payoff

$$\Pi_i(b_i, P_{gi}^{\text{opt}}(b)) := P_{gi}^{\text{opt}}(b) b_i - C_i(P_{gi}^{\text{opt}}(b)). \tag{8}$$

For an unbounded optimizer we have $\Pi_i(b_i, \pm\infty) = -\infty$. To analyze the clearing of the market, we resort to tools from game theory [18]. To this end, we define the *inelastic electricity market game*:

- Players: the set of generators $[n]$.
- Action: for each player $i \in [n]$, the bid $b_i \in \mathbb{R}$.
- Payoff: for each player $i \in [n]$, the payoff Π_i in (8).

For the bid vector we interchangeably use the notation $b \in \mathbb{R}^n$ and $(b_i, b_{-i}) \in \mathbb{R}^n$, where b_{-i} represents the bids of all players except i. A bid profile $b^* \in \mathbb{R}^n$ is a *Nash equilibrium* if there exists an optimizer $P_g^{\text{opt}}(b^*)$ of (7) such that $\forall i \in [n]$,

$$\Pi_i(b_i, P_{gi}^{\text{opt}}(b_i, b_{-i}^*)) \leq \Pi_i(b_i^*, P_{gi}^{\text{opt}}(b^*))$$

for all $b_i \neq b_i^*$ and all optimizers $P_{gi}^{\text{opt}}(b_i, b_{-i}^*)$ of (7). In particular, we are interested in bid profiles that can be associated to economic dispatch. More specifically, a bid $b^* \in \mathbb{R}^n$ is *efficient* is a bid if there exists an optimizer P_g^* of (6) which is also an optimizer of (7) given bids $b = b^*$ and

$$P_{gi}^* = \arg\max_{P_{gi}} \{P_{gi} b_i^* - C_i(P_{gi})\} \text{ for all } i \in [n]. \tag{9}$$

A bid b^* is an *efficient Nash equilibrium* if it is both efficient and a Nash equilibrium. At the efficient Nash equilibrium, the optimal generation allocation determined by (6) coincides with the production that the generators are willing to provide, maximizing their profit (8). Following the same arguments as in the proof of [17, Lemma 3.2], one can establish the existence and uniqueness of the efficient Nash equilibrium.

Proposition III.1. *(Existence and uniqueness of efficient Nash equilibrium): Let (P_g^*, λ^*) be a primal-dual optimizer of (6), then $b^* = \nabla C(P_g^*) = \mathbb{1}\lambda^*$ is the unique efficient Nash equilibrium of the inelastic electricity market game.*

In the scenario described above, neither the ISO nor the individual strategic generators are able to determine the efficient Nash equilibrium beforehand. Our goal is then to design an online bidding algorithm where ISO and generators iteratively exchange information about the bids and the generation quantities before the market is cleared and dispatch commands are sent. The algorithm should be truly implementable, meaning that it should account for the discrete nature of the bidding process, and at the same time ensure that network frequency, governed by the continuous-time power system dynamics, is regulated to its nominal value. The combination of these two aspects leads us to adopt a hybrid implementation strategy to tackle the problem.

IV. Robustness of the continuous-time bid and power-setpoint update scheme

In this section, we introduce a continuous-time dynamics that prescribes a policy for bid updates paired with the frequency dynamics of the power network whose equilibrium corresponds to an efficient Nash equilibrium and zero frequency deviation. In this scheme, generators update their bids in a decentralized fashion based on the power generation quantities received by the ISO, while the ISO changes the generation quantities depending on both the generator bids and the network frequency. This design is a simplified version of the one proposed in our previous work [14]. The main contribution of our treatment here is the identification of a novel Lyapunov function that, beyond helping establish local exponential convergence, allows us to characterize the input-to-state stability properties of the dynamics. We build on this characterization later to develop our time-triggered hybrid implementation that solves the problem outlined in Section III.

A. Bidding process coupled with physical network dynamics

Recall from Section III that given bid b_i, generator $i \in [n]$ wants to produce the amount of power that maximizes its individual profit, given by

$$P_{gi}^{\text{des}} := \arg\max_{P_{gi}} \{b_i P_{gi} - C_i(P_{gi})\} = q_i^{-1}(b_i - c_i) \tag{10}$$

Hence, if the ISO wants generator i to produce more power than its desired quantity, that is $P_{gi} > P_{gi}^{\text{des}}$, generator i will increase its bid, and vice versa. Bearing this rationale in mind, the generators update their bids according to

$$T_b \dot{b} = P_g - Q^{-1} b + Q^{-1} c. \tag{11a}$$

Here $T_b \in \mathbb{R}^{n \times n}$ is a diagonal positive definite matrix. Next, we provide an update law for the ISO depending on the bid

$b \in \mathbb{R}^n$ and the local frequency of the power network. The ISO updates its actions according to

$$\begin{aligned} T_g \dot{P}_g &= \mathbb{1}\lambda - b + \rho \mathbb{1}\mathbb{1}^T (P_d - P_g) - \sigma^2 \omega \\ \tau_\lambda \dot{\lambda} &= \mathbb{1}^T (P_d - P_g) \end{aligned} \tag{11b}$$

with parameters $\rho, \sigma, \tau_\lambda \in \mathbb{R}_{>0}$ and where $T_g \in \mathbb{R}^{n \times n}$ is a diagonal positive definite gain matrix.

The intuition behind the dynamics (11b) is explained as follows. If generator i bids higher than the Lagrange multiplier λ (sometimes referred to as the *shadow price* [19]) associated to (7b), then the power generation (setpoint) of node i is decreased, and vice versa. By adding the term with $\rho > 0$, one can enhance the convergence rate of (11b), see e.g., [20]. We add the feedback signal $-\sigma^2\omega$ to compensate for the frequency deviations in the physical system. Interestingly, albeit we do not pursue this here, the dynamics (11) could also be implemented in a distributed way without the involvement of a central regulating authority like the ISO.

For the remainder of the paper, we assume that there exists an equilibrium $\bar{x} = \mathrm{col}(\bar{\varphi}, \bar{\omega}, \bar{b}, \bar{P}_g, \bar{\lambda})$ of (3)-(11) such that $D^T D_t^{\dagger T} \bar{\varphi} \in (-\pi/2, \pi/2)^m$ (cf. Section II). Note that this equilibrium satisfies

$$\begin{aligned} &\bar{\lambda} = \frac{\mathbb{1}^T (P_d + Q^{-1} c)}{\mathbb{1}^T Q^{-1} \mathbb{1}} > 0, \qquad \bar{\omega} = 0, \quad \bar{b} = \mathbb{1}\bar{\lambda}, \\ &\bar{P}_g = Q^{-1}\mathbb{1}\bar{\lambda} - Q^{-1} c, \qquad \mathbb{1}^T \bar{P}_g = \mathbb{1}^T P_d. \end{aligned} \tag{12}$$

In particular, at the steady state, the frequency deviation is zero, the power balance $\mathbb{1}^T \bar{P}_g = \mathbb{1}^T P_d$ is satisfied, and $\mathbb{1}\bar{\lambda} = \bar{b} = \nabla C(\bar{P}_g)$, implying that $\bar{P}_g$ is a primal optimizer of (6) and $\bar{b}$ is an efficient Nash equilibrium by Proposition III.1. Hence, at steady state the generators do not have any incentive to deviate from the equilibrium bid.

B. Local input-to-state (LISS) stability

While the ISO dynamics (11b) is a saddle-point dynamics of the linear optimization problem (7) (and hence, potentially unstable), we show next that the interconnection of the physical power network dynamics (3) with the bidding process (11) is locally exponentially stable and, furthermore, robust to additive disturbances. For $x = \mathrm{col}(\varphi, \omega, b, P_g, \lambda)$, define the function

$$\begin{aligned} V(x) = U(\varphi) - (\varphi - \bar{\varphi})^T \nabla U(\bar{\varphi}) - U(\bar{\varphi}) + \tfrac{1}{2}\omega^T M \omega \\ + \tfrac{1}{2\sigma^2}(\|b - \bar{b}\|^2_{T_b} + \|P_g - \bar{P}_g\|^2_{T_g} + \|\lambda - \bar{\lambda}\|^2_{\tau_\lambda}). \end{aligned} \tag{13}$$

Then the closed-loop system obtained by combining (3) and (11) is compactly written as

$$\dot{x} = F(x) = \mathcal{Q}^{-1} \mathcal{A} \mathcal{Q}^{-1} \nabla V(x) \tag{14}$$

with $\mathcal{Q} = \mathcal{Q}^T = \mathrm{blockdiag}(I, M, \frac{T_b}{\sigma}, \frac{T_g}{\sigma}, \frac{\tau_\lambda}{\sigma}) > 0$ and

$$\mathcal{A} = \begin{bmatrix} 0 & D_t^T & 0 & 0 & 0 \\ -D_t & -A & 0 & \sigma I & 0 \\ 0 & 0 & -Q^{-1} & I & 0 \\ 0 & -\sigma I & -I & -\rho \mathbb{1}\mathbb{1}^T & \mathbb{1} \\ 0 & 0 & 0 & -\mathbb{1}^T & 0 \end{bmatrix}.$$

By exploiting the structure of the system, we obtain the dissipation inequality

$$\dot{V} = \frac{1}{2}(\nabla V(x))^T \mathcal{Q}^{-1} (\mathcal{A} + \mathcal{A}^T) \mathcal{Q}^{-1} \nabla V(x) \leq 0 \tag{15}$$

However, since $\mathcal{R} := -\frac{1}{2}(\mathcal{A} + \mathcal{A}^T)$ is only positive semi-definite, V is not strictly decreasing along the trajectories of (14). Nevertheless, one can invoke the LaSalle Invariance Principle to characterize the local asymptotic convergence properties of the dynamics, cf. [14]. Here, we show that, in fact, the dynamics is locally input-to-state (LISS) stable, as defined in [21], and therefore robust to additive disturbances. Our key tool to establish this is the identification of a LISS-Lyapunov function, which in general is far from trivial for dynamics that involve saddle-point dynamics. To this end, consider the system

$$\dot{x} = F(x) + Bd \tag{16}$$

with $B \in \mathbb{R}^{4n \times q}$ and a disturbance signal $d \in \mathbb{R}^q$. In the following result, we use the function V to construct an LISS-Lyapunov function for the system (16).

Theorem IV.1. *(LISS-Lyapunov function for the interconnected dynamics): Consider the interconnected dynamics* (16) *and define the function*

$$\begin{aligned} W_\epsilon(x) = V(x) + \epsilon_0 \epsilon_1 (\varphi - \bar{\varphi})^T D_t^\dagger M \omega \\ - \tfrac{\epsilon_0 \epsilon_2}{\sigma^2}(b - \bar{b})^T T_g (P_g - \bar{P}_g) - \tfrac{\epsilon_0 \epsilon_3}{\sigma^2}(\lambda - \bar{\lambda}) \mathbb{1}^T T_g (P_g - \bar{P}_g), \end{aligned} \tag{17}$$

with parameters $\epsilon = \mathrm{col}(\epsilon_0, \epsilon_1, \epsilon_2, \epsilon_3) \in \mathbb{R}^4_{>0}$ and V given by (13)*. Given the equilibrium $\bar{x} = \mathrm{col}(\bar{\varphi}, \bar{\omega}, \bar{b}, \bar{P}_g, \bar{\lambda})$ of* (14)*, let $\bar{\eta} = D^T D_t^{\dagger T} \bar{\varphi}$. For γ such that $\|\bar{\eta}\|_\infty < \gamma < \frac{\pi}{2}$, define the closed convex set*

$$\Omega = \{x = \mathrm{col}(\varphi, \omega, b, P_g, \lambda) \mid D^T D_t^{\dagger T} \varphi \in [-\gamma, \gamma]^m\}. \tag{18}$$

Then there exist sufficiently small ϵ such that W_ϵ is an LISS-Lyapunov function of (16) *on Ω. In particular, there exist constants $\alpha, \chi, c_1, c_2 > 0$ such that for all $x \in \Omega$ and all d satisfying $\|d\| \leq \chi \|x - \bar{x}\|$,*

$$\tfrac{1}{2} c_1 \|x - \bar{x}\|^2 \leq W_\epsilon(x) \leq \tfrac{1}{2} c_2 \|x - \bar{x}\|^2, \tag{19a}$$

$$(\nabla W_\epsilon(x))^T (F(x) + Bd) \leq -\alpha \|x - \bar{x}\|^2. \tag{19b}$$

We refer to Appendix A for the proof of Theorem IV.1. Using the characterization (19) and [22, Theorem 4.10], each trajectory of (14) initialized in a compact level set contained in Ω exponentially converges to the equilibrium $\bar{x}$ corresponding to economic dispatch and the efficient Nash equilibrium. Moreover, we exploit the local ISS property of (16) guaranteed by Theorem IV.1 next to develop a time-triggered hybrid implementation.

V. Time-triggered implementation: iterative bid update and market clearing

In realistic implementations, the bidding process between the ISO and the generators is not performed continuously. Given the availability of digital communications, it is reasonable to instead model it as an iterative process. Building on the continuous-time bidding dynamics proposed in Section IV,

here we develop a time-triggered hybrid implementation that combines the discrete nature of bidding with the continuous nature of the frequency evolution in the power network. We consider two time-scales, one (faster) for the bidding process that incorporates at each step the frequency measurements, and another one (slower) for the market clearing and updates of the power generation levels that are sent to the power network dynamics. We refer to this implementation as time-triggered because we do not necessarily prescribe the time schedules to be periodic in order to guarantee that the asymptotic stability properties are retained by the hybrid implementation.

A. Algorithm description

We start with an informal description of the iterative update scheme between the ISO and the generators, and the interconnection with the dynamics of the power network.

> *[Informal description]:* The algorithm has two time indices, k to label the iterations on the bidding process and l to label the iteration in the market clearing process that updates the power setpoints. At each iteration $l \in \mathbb{Z}_{\geq 0}$, ISO and generators are involved in an iterative process where, at each subiteration k, generators send a bid to the ISO. Once the ISO has obtained the bids and the network frequency measurements at time t_k^l, it computes the new potential generation allocations, denoted $P_g^{k+1} \in \mathbb{R}^n$, and sends the corresponding one to each generator. At the $(k+1)$-th subiteration, each generator adjust its bid based on their previous bid and the generation allocation received from the ISO at time t_{k+1}^l. Once $k = N_l \in \mathbb{Z}_{\geq 1}$ at time $t_{N_l}^l$, the market is cleared, meaning that the bidding process is reset (i.e., $k = 0$), the power generations in the swing equations are updated according to the current setpoints $P_g^{N_l}$, and the index l moves to $l+1$.

Figure 1 shows the two iteration layers in the update scheme. The evolution of the frequency occurs in continuous time according to (3). To relate iteration numbers with time instances on $\mathbb{R}$, we consider time sequences of the form $\{\{t_k^l\}_{k=0}^{N_l}\}_{l=0}^{\infty}$ for $N_l \in \mathbb{Z}_{\geq 1}$ and $l \in \mathbb{Z}_{\geq 0}\}$, satisfying

$$t_k^l - t_{k-1}^l > 0, \qquad t_0^{l+1} = t_{N_l}^l \tag{20}$$

for all $l \in \mathbb{Z}_{\geq 0}$ and all $k \in [N_l]$. Algorithm 1 formally describes the iterative updates of the bidding process between the generators and the ISO.

For analysis purposes, we find it convenient to represent the dynamics resulting from the combination of Algorithm 1 and the network dynamics (3) as the time-triggered continuous-time system

$$\begin{aligned}
\dot{\varphi}(t) &= D_t^T \omega(t),\\
M\dot{\omega}(t) &= -D_t \nabla U(\varphi(t)) - A\omega(t) + P_g(t_0^l) - P_d,\\
T_b \dot{b}(t) &= P_g(t_k^l) - Q^{-1} b(t_k^l) - Q^{-1} c,\\
T_g \dot{P}_g(t) &= \mathbb{1}\lambda(t_k^l) - b(t_k^l) - \sigma^2 \omega(t_k^l) + \rho \mathbb{1}\mathbb{1}^T (P_d - P_g(t_k^l)),\\
\tau_\lambda \dot{\lambda}(t) &= \mathbb{1}^T (P_d - P_g(t_k^l)),
\end{aligned} \tag{21}$$

Algorithm 1: ITERATIVE BID UPDATE AND MARKET CLEARING ALGORITHM

Executed by: generators $i \in [n]$ and ISO
Data : time sequence $\{\{t_k^l\}_{k=0}^{N_l}\}_{l=0}^{\infty}$; cost function (4) for each generator i; frequency deviation $\omega(t_k^l)$ at each time t_k^l and load P_d for ISO
Initialize : each generator i selects arbitrarily $b_i^0 \geq c_i$, sets $k = 0, l = 0$, and jumps to step 6; ISO selects arbitrary $P_{gi}^0 > 0, \lambda_i^0 > 0$, sets $k = 0, l = 0$ and waits for step 8

while $l \geq 0$ **do**
  while $k \geq 0, k < N_l$ **do**
    /* For each generator i: */
    Receive P_{gi}^k from ISO at t_k^l; Set $b_i^{k+1} = b_i^k + (t_{k+1}^l - t_k^l) T_{gi}^{-1} (P_{gi}^k - q_i^{-1}(b_i^k + c_i))$
    Send b_i^{k+1} to the ISO; set $k = k+1$
    /* For ISO: */
    Receive $b_i^k, \omega_i(t_k^l)$ from each $i \in [n]$ at t_k^l
    Set $P_{gi}^{k+1} = P_{gi}^k + (t_{k+1}^l - t_k^l) T_{gi}^{-1} (\lambda^k - b_i^k - \sigma^2 \omega_i(t_k^l) + \rho \sum_{i \in [n]} (P_{di} - P_{gi}^k))$ for all $i \in [n]$
    $\lambda^{k+1} = \lambda^k + \frac{t_{k+1}^l - t_k^l}{\tau_\lambda} \sum_{i \in [n]} (P_{di} - P_{gi}^k)$
    Send P_{gi}^{k+1} to each $i \in [n]$, set $k = k+1$
  end
  Set $P_{gi}(t) = P_{gi}^{N_l}$ in (3) $\forall i \in [n], \forall t \in [t_{N_l}^l, t_{N_{l+1}}^{l+1})$
  Set $b_i^0 = b_i^{N_l}, P_{gi}^0 = P_{gi}^{N_l}, \lambda_i^0 = \lambda_i^{N_l}$ for each $i \in [n]$
  Set $l = l+1, k = 0$
end

for $t \in [t_k^l, t_{k+1}^l) \subset [t_0^l, t_0^{l+1}), l \in \mathbb{Z}_{\geq 0}, k \in \{0, \ldots, N_l - 1\}$. We write the system (21) compactly in the form

$$\dot{x}(t) = f(x(t)) + g(x(t_k^l)) + h(x(t_0^l)) \tag{22}$$

with

$$\begin{aligned}
f(x) &= \mathrm{col}(D_t^T \omega, -M^{-1}(D_t \nabla U(\varphi) + A\omega + P_d), 0, 0, 0),\\
g(x) &= \mathrm{col}(0, 0, T_b^{-1}(P_g - Q^{-1} b - Q^{-1} c),\\
&\quad T_g^{-1}(\mathbb{1}\lambda - b - \sigma^2 \omega + \rho \mathbb{1}\mathbb{1}^T (P_d - P_g)), \tau_\lambda^{-1} \mathbb{1}^T (P_d - P_g)),\\
h(x) &= \mathrm{col}(0, M^{-1} P_g, 0, 0, 0).
\end{aligned}$$

With this notation, note that the continuous-time dynamics (14) corresponds to

$$\dot{x}(t) = f(x(t)) + g(x(t)) + h(x(t)). \tag{23}$$

Since $\sup_{\varphi \in \mathbb{R}^{n-1}} \|\nabla^2 U(\varphi)\| < \infty$ and g, h are linear, it follows that f, g, h are globally Lipschitz (we denote by L_f, L_g, L_h their Lipschitz constants, respectively). When viewed as a continuous-time system, the dynamics (21) has a discontinuous right-hand side, and therefore we consider its solutions in the Carathéodory sense, cf. [23].

B. Sufficient condition on triggering times for stability

In this section we establish conditions on the time sequence that guarantee that the solutions of (21) are well-defined and

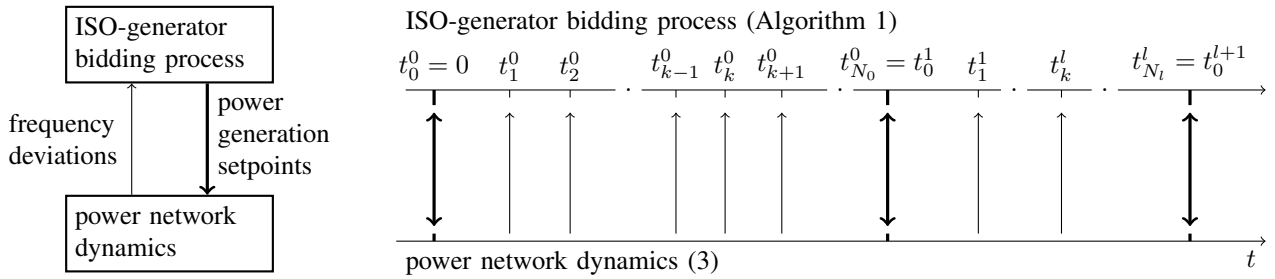

Figure 1: Relation between time and iteration numbers in the time-triggered system (21). The lower time-axis corresponds to the continuous-time physical system (3) while the upper one corresponds to the time sequence $\{\{t_k^l\}_{k=0}^{N_l}\}_{l=0}^{\infty}$ of the ISO-generator bidding process given in Algorithm 1. The arrows pointing up indicate the frequency updates in the bidding dynamics while the arrows pointing down correspond to update of the power generation levels in the physical system. As indicated, for each $l \in \mathbb{Z}_{\geq 0}$ the lower index k is reset once it reaches $k = N_l \in \mathbb{Z}_{\geq 1}$, i.e., $t_{N_l}^l = t_0^{l+1}$ for all $l \in \mathbb{Z}_{\geq 0}$.

retain the convergence properties of (14). Specifically, we determine a sufficient condition on the inter-sampling times $t_{k+1}^l - t_k^l$ for bidding and $t_k^{l+1} - t_k^l$ for market clearing that ensure local asymptotic convergence of (22) to the equilibrium $\bar{x}$ of the continuous-time system (14).

Our strategy to accomplish this relies on the robustness properties of (14) characterized in Theorem IV.1 and the fact that the time-triggered implementation, represented by (22), can be regarded as an approximation of the continuous-time dynamics, represented by (23). We use the Lyapunov function W_ϵ defined by (17) and examine the mismatch between both dynamics to derive upper bounds on the inter-event times that guarantee that W_ϵ is strictly decreasing along the time-triggered system (21).

Theorem V.1. *(Local asymptotic stability of time-triggered implementation): Consider the time-triggered implementation* (21) *of the interconnection between the ISO-generator bidding processes and the power network dynamics. With the notation of Theorem IV.1, let*

$$\bar{\xi} := \frac{1}{L_f + L_g} \log\Big(1 + \frac{\beta(L_f + L_g)}{L(L_W L_h + \beta)}\Big), \tag{24}$$
$$\bar{\zeta} := \frac{1}{L_f} \log\Big(1 + \frac{L_f(\alpha - \beta)}{L_g(LL_W + \alpha) + (\alpha - \beta)(L_f + L_g)}\Big),$$

where $0 < \beta < \alpha$, $L := L_f + L_g + L_h$, *and* L_W *is the Lipschitz constant of* ∇W_ϵ. *Assume the time sequence* $\{\{t_k^l\}_{k=0}^{N_l}\}_{l=0}^{\infty}$ *satisfies, for some* $\underline{\zeta} \in (0, \bar{\zeta})$ *and* $\underline{\xi} \in (0, \bar{\xi})$,

$$\underline{\zeta} \leq t_0^{l+1} - t_0^l \leq \bar{\zeta} \quad \text{and} \quad \underline{\xi} \leq t_k^l - t_{k-1}^l \leq \bar{\xi}, \tag{25}$$

for all $l \in \mathbb{Z}_{\geq 0}$ *and* $k \in [N_l]$. *Then,* $\bar{x}$ *is locally asymptotically stable under* (21).

We refer the reader to Appendix B for the proof of Theorem V.1. The uniform lower bounds $\underline{\zeta}$ and $\underline{\xi}$ in (25) ensure that the solutions of the time-triggered implementation (21) are well-defined, avoiding Zeno behavior. Theorem V.1 implies that convergence is guaranteed for any constant stepsize implementation, where the sufficiently small stepsize satisfies (25). However, the result of Theorem V.1 is more general and does not require constant stepsizes. Another interesting observation is that the upper bounds can be calculated without requiring any information about the equilibrium $\bar{x}$. This is desirable, as this equilibrium is not known beforehand and must be determined by the algorithm itself.

VI. Simulations

In this section we illustrate the convergence properties of the interconnected time-triggered system (21). We consider the IEEE 14-bus power network depicted in Figure 2, where each node has one generator and one load according to model (1). We assume costs at each node $i \in [14]$ of the form

$$C_i(P_{gi}) = \frac{1}{2} q_i P_{gi}^2 + c_i P_{gi}$$

with $q_i > 0$ and $c_i \geq 0$. In the original IEEE 14-bus benchmark model, nodes $1, 2, 3, 6, 8$ have synchronous generators while the other nodes are load nodes and have no power generation. We replicate this by suitably choosing the cost at the load nodes such that the optimizer of the economic dispatch problem (6) is zero at them. In addition, we choose $M_i \in [4, 5.5]$ for generator nodes $i \in \{1, 2, 3, 6, 8\}$ and $M_i \ll 1$ for the load nodes. We set $A_i \in [1.5, 2.5], V_i \in [1, 1.06], T_{bi} \in [0.0005, 0.001], T_{gi} = 13.5$ for all $i \in [14]$ and $\rho = 900$. The other parameter values for the ISO dynamics (11b) are $\tau_\lambda = 0.0004$, $\rho = 3$, $\sigma = 17$.

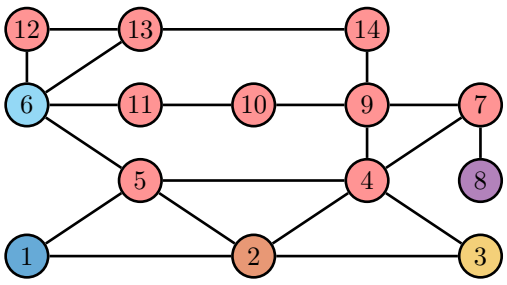

Figure 2: Schematic of the modified IEEE 14-bus benchmark. Each edge represents a transmission line. Red nodes represent loads. All the other nodes represent synchronous generators, with different colors that match the ones used in Figures 3 and 5. The physical dynamics are modeled by (1).

At time $t = 0$ s, the load (in MW's) is given by

$$P_d = (0, 20, 86, 43, 7, 10, 0, 0, 27, 8, 3, 6, 12, 14).$$

Initially, we set $(q_1, q_2, q_3, q_6, q_8) = (22, 128, 45, 60, 30)$, $(c_1, c_2, c_3, c_6, c_8) = (7.5, 7.5, 7.5, 7.5, 7.5)$ and $q_i = 1500, c_i = 26$ for the remaining nodes. The time-triggered

system (21) is initialized at steady state at the optimal generation level

$$(P_{g1}, P_{g2}, P_{g3}, P_{g6}, P_{g8}) = (85, 15, 42, 31, 63)$$

and with $P_{gi} = 0$ for all other nodes. Figures 3-5 depict the simulation of the time-triggered system for different triggering times. At $t = 1\,\mathrm{s}$ all the loads are increased by 10% and we set $c_i = 28$ for the load nodes. As observed in all figures, the trajectories converge to a new efficient equilibrium with optimal power generation level

$$(P_{g1}, P_{g2}, P_{g3}, P_{g6}, P_{g8}) = (94, 16, 46, 34, 69)$$

and $P_{gi} = 0$ for all other nodes. Furthermore, at steady state the generators all bid equal to the Lagrange multiplier which, by Proposition III.1, corresponds to an efficient Nash equilibrium.

At $t = 15\,\mathrm{s}$ the cost functions of the generators are changed to $(q_1, q_2, q_3, q_6, q_8) = (23, 116, 48, 63, 38)$, $(c_1, c_2, c_3, c_6, c_8) = (7.5, 6, 13.5, 15, 10.5)$ and $q_i = 1500, c_i = 33$ for the remaining nodes. As a result, the optimal dispatch of power changes. Due to the changes of the power generation, a temporary frequency imbalance occurs. As illustrated in Figures 3-5, the power generations converge to the new optimal steady state given by

$$(P_{g1}, P_{g2}, P_{g3}, P_{g6}, P_{g8}) = (108, 23, 40, 28, 60).$$

In addition, we observe that after each change of either the load or the cost function, the frequency is stabilized and the bids converge to a new efficient Nash equilibrium. The fact that the frequency transients are better in Figures 3-4 (with inter-event times of maximal 2 ms for bidding and on average respectively 50 ms, 62.5 ms for market clearing) than in Figure 5 (with inter-event times of 2 ms for bidding and 160 ms for market clearing) is to be expected given the longer inter-event times in the second case. A slight increase in the inter-event times for Figure 5 in either bid updating or market clearing time result in an unstable system. Figure 6 illustrates the evolution of the interconnected system with the primary/secondary and tertiary control layers separated and its loss of efficiency compared to the proposed integrated design.

VII. Conclusions

This paper has studied the joint operation of the economic dispatch and frequency regulation layers, which are traditionally separated in the control of power networks. The starting point of our design was a continuous-time bid update scheme coupled with the frequency dynamics whose equilibrium corresponds to an efficient Nash equilibrium and zero frequency deviation. Building on the identification of a novel LISS-Lyapunov function for this dynamics, we have characterized its robustness properties against additive disturbances. We have exploited the LISS-property to propose a provably correct multi-rate hybrid implementation that combines the iterative nature of the fast bid updates and the slower power setpoint updates with the continuous frequency network dynamics. Our results show that real-time iterative bidding can successfully be interconnected with frequency control to increase efficiency while retaining stability of the power system.

Future work will incorporate elastic demand, generator bounds, and power flow constraints in the formulation, develop distributed and opportunistic self-triggered implementations of the proposed dynamics, and characterize the convergence properties of data-driven optimization algorithms.

Appendix A
Proof of Theorem IV.1

We structure the proof of Theorem IV.1 in two separate parts, corresponding to the inequalities (19a) and (19b), respectively.

A. Positive definiteness of Lyapunov function W_ϵ

Let $\bar{x}$ be the equilibrium of (14) satisfying the hypothesis. We now prove the existence of constants $c_1, c_2, \epsilon_0 > 0$ such that (19a) holds, given the constants $\epsilon_1, \epsilon_2, \epsilon_3 > 0$. The Hessian of W_ϵ (eq. (17)) is given by a block-diagonal matrix $\nabla^2 W_\epsilon(x) = \mathrm{blockdiag}(H_1(\varphi), H_2)$ with the upper left block given by

$$H_1(\varphi) = \begin{bmatrix} \nabla^2 U(\varphi) & \epsilon_0\epsilon_1 D_t^\dagger M \\ \epsilon_0\epsilon_1 M D_t^{\dagger T} & M \end{bmatrix}$$

and the lower right block is given by

$$H_2 = \frac{1}{\sigma^2}\begin{bmatrix} T_b & -\epsilon_0\epsilon_2 T_g & 0 \\ -\epsilon_0\epsilon_2 T_g & T_g & -\epsilon_0\epsilon_3 T_g \mathbb{1} \\ 0 & -\epsilon_0\epsilon_3 \mathbb{1}^T T_g & \tau_\lambda \end{bmatrix}.$$

We will now show that there exists sufficiently small ϵ_0 such that $H_1(\varphi), H_2$ are both positive definite for all $x \in \Omega$. To this end, let us define the function

$$\mathcal{U}(\eta) = D_t^\dagger D \Gamma \cos(\eta) D^T D_t^{\dagger T} \tag{26}$$

and note that $\mathcal{U}(D^T D_t^{\dagger T}\varphi) = \nabla^2 U(\varphi)$, implying that $0 < \mathcal{U}(\gamma\mathbb{1}) \le \nabla^2 U(\varphi) \le \nabla^2 U(0) = \mathcal{U}(0)$ for all $x \in \Omega$, see (18). Consequently, for $\mathcal{D} := \epsilon_0\epsilon_1 D_t^\dagger M$, we have

$$\underbrace{\begin{bmatrix} \mathcal{U}(\gamma\mathbb{1}) & \mathcal{D} \\ \mathcal{D}^T & M \end{bmatrix}}_{K_1} \le H_1(\varphi) \le \underbrace{\begin{bmatrix} \mathcal{U}(0) & \mathcal{D} \\ \mathcal{D}^T & M \end{bmatrix}}_{K_2}, \qquad \forall x \in \Omega.$$

By considering the Schur complements, the matrices K_1, H_2 are shown to be positive definite by choosing $\epsilon_0 > 0$ sufficiently small such that

$$\begin{aligned} \mathcal{U}(\gamma\mathbb{1}) - \epsilon_0^2\epsilon_1^2 D_t^\dagger M D_t^{\dagger T} > 0, \\ T_b - \epsilon_0^2\epsilon_2^2 T_g > 0, \\ \tau_\lambda - \epsilon_0^2\epsilon_3^2 \mathbb{1}^T T_b T_g (T_b - \epsilon_0^2\epsilon_2^2 T_g)^{-1}\mathbb{1} > 0. \end{aligned} \tag{27}$$

Next we define

$$c_1 := \min\{\lambda_{\min}(K_1), \lambda_{\min}(H_2)\}, \tag{28}$$

$$c_2 := \max\{\lambda_{\max}(K_2), \lambda_{\max}(H_2)\}, \tag{29}$$

where $\lambda_{\min}(A), \lambda_{\max}(A)$ denote the smallest and largest eigenvalue of the matrix $A \in \mathbb{R}^{n\times n}$. Note that $c_1, c_2 > 0$ and the following holds

$$0 < c_1 I \le \nabla^2 W_\epsilon(x) \le c_2 I, \qquad \forall x \in \Omega \tag{30}$$

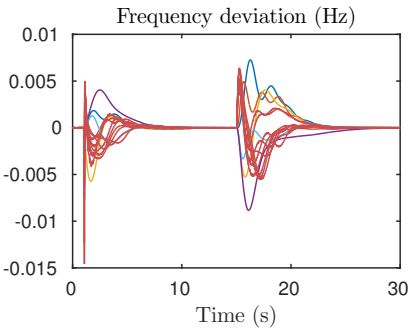

(a) Evolution of the frequency deviations. After each sudden supply-demand imbalance, frequency is restored to its nominal value.

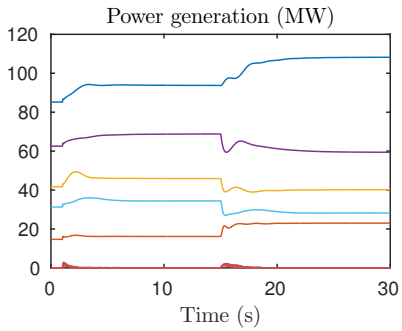

(b) Evolution of the nodal power generations. After each change in the network, the power generation quantities converge to the optimal values determined by (6).

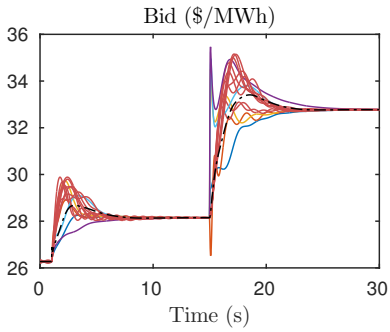

(c) Evolution of the bids and the Lagrange multiplier (dashed black line). As shown, the bids converge to the unique efficient Nash equilibrium.

Figure 3: Simulations of the interconnection between the iterative bidding mechanism and the power network dynamics modeled by the time-triggered system (21). The colors in the graph corresponds to the nodes as depicted in Figure 2. We choose identical inter-event times given by $t_k^l - t_{k-1}^l = 2\,\text{ms}, t_0^l - t_0^{l-1} = 50\,\text{ms}$ for all $l \in \mathbb{Z}_{\geq 1}, k \in [25]$. As expected, the time-triggered system is asymptotically stable for sufficiently fast updates.

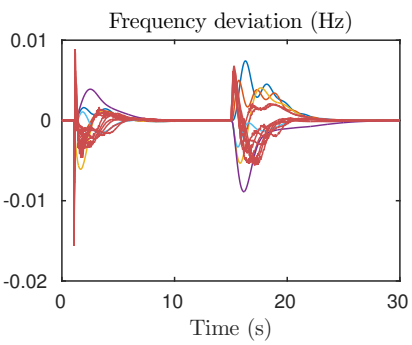

(a) Evolution of the frequency deviations.

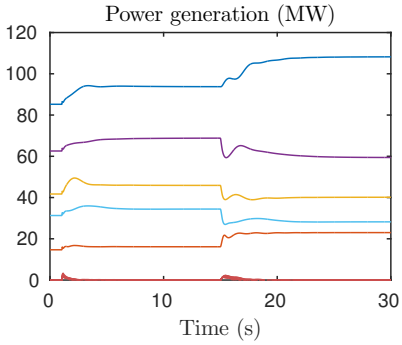

(b) Evolution of each power generation.

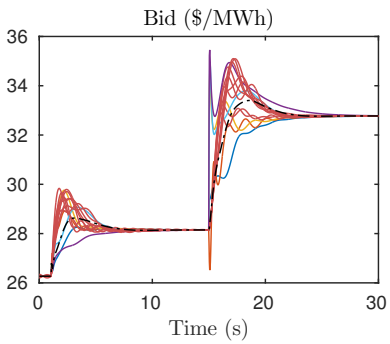

(c) Evolution of the bids & Lagrange multiplier.

Figure 4: Simulations of the time-triggered system (21) under time-varying step sizes. We choose the time between two consecutive bid iterations randomly between $0.5\,\text{ms} \leq t_k^l - t_{k-1}^l \leq 2\,\text{ms}$, for all $l \in \mathbb{Z}_{\geq 1}, k \in [N_l]$, and we choose the number of bid iterations $N_l \in \mathbb{Z}$ before market clearing occurs randomly in the interval $[20, 80]$. Since the step sizes are sufficiently small, and therefore the mismatch of the time-triggered system with its continuous-time variant, the performance is similar compared to Figure 3.

Note that since $W_\epsilon(\bar{x}) = 0, \nabla W_\epsilon(\bar{x}) = 0$, we have

$$\begin{aligned} W_\epsilon(x) &= W_\epsilon(x) - W_\epsilon(\bar{x}) \\ &= (x-\bar{x})^T \int_0^1 \Big(\nabla W_\epsilon((x-\bar{x})T + \bar{x}) - \nabla W_\epsilon(\bar{x})\Big) dT \\ &= (x-\bar{x})^T \int_0^1 \int_0^1 T\nabla^2 W_\epsilon((x-\bar{x})T\theta + \bar{x}) dT d\theta (x-\bar{x}). \end{aligned}$$

Since Ω is convex, it follows that $xT\theta + (1-T\theta)\bar{x} \in \Omega$ for all $T, \theta \in [0,1], x \in \Omega$. Consequently, by (30) we have

$$c_1 I \leq \nabla^2 W_\epsilon(xT\theta + (1-T\theta)\bar{x}) \leq c_2 I, \ \forall T, \theta \in [0,1],$$

and $\forall x \in \Omega$. Since $\int_0^1 \int_0^1 T d\theta dT = \frac{1}{2}$, inequality (19a) follows.

B. Dissipation inequality

Here we establish the inequality (19b). First we consider the case without disturbance, i.e., $d = 0$. Given the equilibrium $\bar{x}$ of (14), we define $\tilde{x} := x - \bar{x}$ and likewise $\tilde{\varphi}, \tilde{\omega}, \tilde{b}, \tilde{P}_g, \tilde{\lambda}$. Then, the system (14) reads as

$$\begin{aligned} \dot{\tilde{\varphi}} &= D_t^T \tilde{\omega}, \\ M\dot{\tilde{\omega}} &= -D_t(\nabla U(\varphi) - \nabla U(\bar{\varphi})) - A\tilde{\omega} + \tilde{P}_g, \\ T_b \dot{\tilde{b}} &= \tilde{P}_g - Q^{-1}\tilde{b}, \\ T_g \dot{\tilde{P}}_g &= \mathbb{1}\tilde{\lambda} - \tilde{b} - \rho \mathbb{1}\mathbb{1}^T \tilde{P}_g - \sigma^2 \tilde{\omega}, \\ \tau_\lambda \dot{\tilde{\lambda}} &= -\mathbb{1}^T \tilde{P}_g. \end{aligned}$$

In addition, note that W_ϵ (eq. (17)) takes the form

$$W_\epsilon(x) = V(x) + V_\epsilon(x), \tag{31}$$

$$V_\epsilon(x) = \epsilon_0\epsilon_1 \tilde{\varphi}^T D_t^\dagger M\omega - \frac{\epsilon_0\epsilon_2}{\sigma^2}\tilde{b}^T T_g \tilde{P}_g - \frac{\epsilon_0\epsilon_3}{\sigma^2}\tilde{\lambda}\mathbb{1}^T T_g \tilde{P}_g. \tag{32}$$

Next, we determine the time-derivative of the individual terms of the candidate Lyapunov function W_ϵ.

(0): First, observe from (15) that

$$\begin{aligned} \dot{V} = &-\omega^T A\omega - \frac{1}{\sigma^2}(b-\bar{b})^T Q^{-1}(b-\bar{b}) \\ &- \frac{\rho}{\sigma^2}(P_g - \bar{P}_g)^T \mathbb{1}\mathbb{1}^T (P_g - \bar{P}_g). \end{aligned}$$

(1): The time-derivative of the first term of V_ϵ satisfies

$$\frac{d}{dt}\tilde{\varphi}^T D_t^\dagger M\omega = \tilde{\omega}^T M D_t^{\dagger T} D_t^T \tilde{\omega}$$

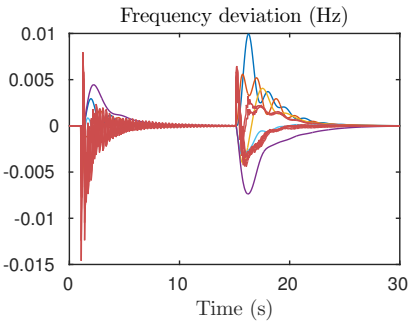

(a) Compared to Figure 3a, there are more oscillations and a larger overshoot of the frequency deviations.

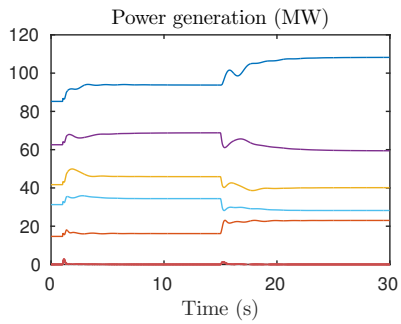

(b) Evolution of the power generations at each node.

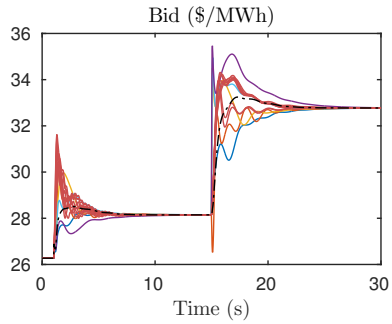

(c) Evolution of the bids and the Lagrange multiplier. Compared to Figure 3c, more oscillations in the bids occur.

Figure 5: Simulations of the time-triggered system (21). Here we consider the case $t_k^l - t_{k-1}^l = 2\,\text{ms}, t_0^l - t_0^{l-1} = 160\,\text{ms}$ for all $l \in \mathbb{Z}_{\geq 1}, k \in [80]$. The scenario is the same as in Figure 3. In this case however, the interconnected time-triggered system is only marginally stable; a small increase in either of the inter-event times results in an unstable system.

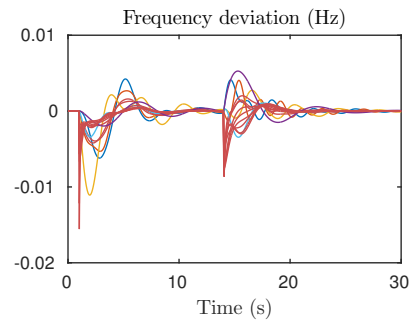

(a) Evolution of the frequency deviations. Compared to Figures 3a-4a, there are more oscillations in the frequency deviations.

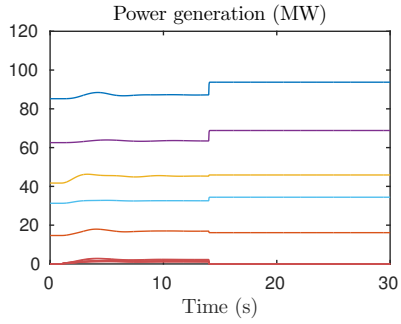

(b) Evolution of each power generation. After primary and secondary controllers are activated at $t = 1\,\text{s}$, optimal power sharing is lost.

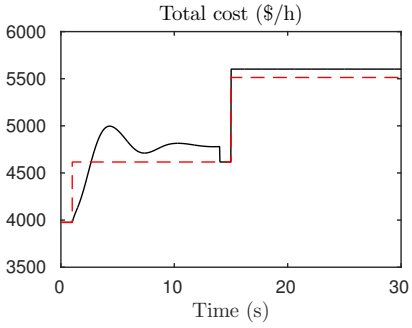

(c) Evolution of the total generation costs (in black) compared to the optimal values calculated by (6). Activation of primary/secondary control, and changes in the cost function result in a loss of efficiency.

Figure 6: Simulations of swing equations with the primary/secondary and tertiary control layers separated. At time $t = 1\,\text{s}$, the load is increased as in Figure 3 and decentralized primary/secondary controllers are activated to regulate the frequency but, as a result, optimal power sharing is lost. At $t = 14\,\text{s}$ the tertiary control layer is activated by resetting the setpoints optimally. After the change of the cost functions at $t = 15\,\text{s}$, economic optimality is temporary lost again until the next time the tertiary control layer is activated (typically in the order of minutes).

$$- \tilde{\varphi}^T D_t^\dagger D_t (\nabla U(\varphi) - \nabla U(\bar{\varphi})) - \tilde{\varphi}^T D_t^\dagger A \tilde{\omega} + \tilde{\varphi}^T D_t^\dagger \tilde{P}_g.$$

By exploiting $D_t^\dagger D_t = I$, the second term is rewritten as

$$-\tilde{\varphi}^T D_t^\dagger D_t (\nabla U(\varphi) - \nabla U(\bar{\varphi})) = -\tilde{\varphi}^T \mathcal{U}(\varphi) \tilde{\varphi}^T$$

where we used that $\nabla U(\varphi) - \nabla U(\bar{\varphi}) = \mathcal{U}(\varphi)(\varphi - \bar{\varphi})$ with

$$\mathcal{U}(\varphi) = \int_0^1 \nabla^2 U((\varphi - \bar{\varphi})\theta + \bar{\varphi}) d\theta. \tag{33}$$

Since $\mathcal{U}(\varphi) \geq \mathcal{U}(\mathbb{1}\gamma) = D_t^\dagger D \Gamma \cos(\mathbb{1}\gamma) D^T D_t^{\dagger T}$ (see eq. (26)) for all $x \in \Omega$, we obtain

$$\frac{d}{dt} \tilde{\varphi}^T D_t^\dagger M \omega \leq \tilde{\omega}^T M D_t^{\dagger T} D_t^T \tilde{\omega} - \tilde{\varphi}^T \mathcal{U}(\mathbb{1}\gamma) \tilde{\varphi}^T - \tilde{\varphi}^T D_t^\dagger A \tilde{\omega} + \tilde{\varphi}^T D_t^\dagger \tilde{P}_g.$$

(2): For the second term of V_ϵ the following holds:

$$\frac{d}{dt} \tilde{b}^T T_g \tilde{P}_g = \tilde{P}_g^T T_{gb} \tilde{P}_g - \tilde{P}_g^T T_{gb} Q^{-1} \tilde{b} + \tilde{b}^T \mathbb{1} \tilde{\lambda} - \tilde{b}^T \tilde{b} - \rho \tilde{b}^T \mathbb{1}\mathbb{1}^T \tilde{P}_g - \sigma^2 \tilde{b}^T \tilde{\omega},$$

where we define $T_{gb} := T_g T_b^{-1}$.

(3): Similarly, by defining $T_{g\lambda} := T_g T_\lambda^{-1}$ we obtain

$$\frac{d}{dt} \tilde{\lambda} \mathbb{1}^T T_g \tilde{P}_g = -\tilde{P}_g^T T_{g\lambda} \mathbb{1}\mathbb{1}^T \tilde{P}_g + n\tilde{\lambda}^2 - \tilde{\lambda} \mathbb{1}^T \tilde{b} - \rho n \tilde{\lambda} \mathbb{1}^T \tilde{P}_g - \sigma^2 \tilde{\lambda} \mathbb{1}^T \tilde{\omega}.$$

By combining the above calculations, we can show that the time-derivative of W_ϵ satisfies

$$\dot{W}_\epsilon = \dot{V} + \dot{V}_\epsilon \leq \frac{1}{2} \epsilon_0 (x - \bar{x})^T \mathcal{P}^T \Xi_\epsilon \mathcal{P} (x - \bar{x}).$$

where Ξ_ϵ is given by (34) (see page 10), $\mathcal{P}$ takes the form

$$\mathcal{P} = \begin{bmatrix} 0 & I & 0 & 0 & 0 \\ 0 & 0 & \frac{1}{\sigma} I & 0 & 0 \\ 0 & 0 & 0 & \frac{1}{\sigma} I & 0 \\ 0 & 0 & 0 & 0 & \frac{1}{\sigma} \\ I & 0 & 0 & 0 & 0 \end{bmatrix},$$

and $\mathcal{M} := M D_t^{\dagger T} D_t^T + D_t D_t^\dagger M, \mathcal{T} := T_{g\lambda} \mathbb{1}\mathbb{1}^T + \mathbb{1}\mathbb{1}^T T_{g\lambda}$. Next, we will show that there exists $\epsilon_0, \epsilon_1, \epsilon_2, \epsilon_3 > 0$ such that Ξ_ϵ is positive definite. This can be done by successive use

$$\Xi_\epsilon = \begin{array}{c} \\ \omega \\ \frac{b}{\sigma} \\ \frac{P_g}{\sigma} \\ \frac{\lambda}{\sigma} \\ \varphi \end{array} \begin{array}{c} \begin{array}{ccccc} \omega & \frac{b}{\sigma} & \frac{P_g}{\sigma} & \frac{\lambda}{\sigma} & \varphi \end{array} \\ \begin{bmatrix} \frac{2}{\epsilon_0}A - \epsilon_1\mathcal{M} & -\epsilon_2\sigma I & 0 & -\epsilon_3\sigma\mathbb{1} & \epsilon_1 A D_t^{\dagger T} \\ -\epsilon_2\sigma I & -2\epsilon_2 I + \frac{2}{\epsilon_0}Q^{-1} & -\epsilon_2(Q^{-1}T_{gb} + \rho\mathbb{1}\mathbb{1}^T) & (\epsilon_2-\epsilon_3)\mathbb{1} & 0 \\ 0 & -\epsilon_2(T_{gb}Q^{-1} + \rho\mathbb{1}\mathbb{1}^T) & 2\epsilon_2 T_{gb} + \frac{2}{\epsilon_0}\rho\mathbb{1}\mathbb{1}^T - \epsilon_3\mathcal{T} & -\epsilon_3 n\rho\mathbb{1} & -\epsilon_1\sigma D_t^{\dagger T} \\ -\epsilon_3\sigma\mathbb{1}^T & (\epsilon_2-\epsilon_3)\mathbb{1}^T & -\epsilon_3 n\rho\mathbb{1}^T & 2n\epsilon_3 & 0 \\ \epsilon_1 D_t^\dagger A & 0 & -\epsilon_1\sigma D_t^\dagger & 0 & 2\epsilon_1\mathcal{U}(\mathbb{1}\gamma) \end{bmatrix} \end{array} \tag{34}$$

of the Schur complement. In particular, for $A \in \mathbb{R}^{n\times n}, B \in \mathbb{R}^{n\times m}, C \in \mathbb{R}^{m\times m}, \beta > 0$, recall that

$$\begin{bmatrix} \beta A & B \\ B^T & C \end{bmatrix} > 0 \quad \iff \quad C > 0 \;\;\&\;\; \beta A - BC^{-1}B^T > 0.$$

For successively applying this result to Ξ_ϵ, given by (34), let us first fix $\epsilon_1, \epsilon_3 > 0$. Then ϵ_2 can be chosen sufficiently large such that lower-right 3×3 block submatrix of Ξ_ϵ is positive definite. Then we can choose a $\epsilon_0 > 0$ sufficiently small such that (27) holds and $\Xi_\epsilon > 0$. Here, note that choosing ϵ_0 smaller does not affect the positive definiteness of the lower-right 3×3 block submatrix of Ξ_ϵ. By construction of $\epsilon_0, \epsilon_1, \epsilon_2, \epsilon_3$, there exist constants $c_1, c_2 \in \mathbb{R}_{>0}$ such that (19a) holds for all $x \in \Omega$, see also Section A-A. In addition, for this choice of ϵ we have that $\Xi_\epsilon > 0$ and, as a result, there exists $\hat{\alpha} := \frac{1}{2}\epsilon_0\lambda_{\min}(\mathcal{P}^T\Xi_\epsilon\mathcal{P}) > 0$ such that

$$(\nabla W_\epsilon(x))^T F(x) \le -\hat{\alpha}\|x - \bar{x}\|^2$$

for all $x \in \Omega$. Next, we consider the case when the disturbance is present. Let χ satisfy $0 < \chi < \hat{\alpha}/(L_W\|B\|)$. Then, by exploiting the Lipschitz property of ∇W_ϵ,

$$\begin{aligned} &(\nabla W_\epsilon(x))^T(F(x) + Bd) \le -\hat{\alpha}\|x-\bar{x}\|^2 + \nabla W_\epsilon(x))^T Bd \\ &\le -\hat{\alpha}\|x-\bar{x}\|^2 + L_W\|B\|\|x-\bar{x}\|\|d\| \\ &\le -(\hat{\alpha} - L_W\|B\|\chi)\|x-\bar{x}\|^2 = -\alpha\|x-\bar{x}\|^2 \end{aligned}$$

with $\alpha := \hat{\alpha} - L_W\|B\|\chi) > 0$ and thus (19b) holds. This concludes the proof of Theorem IV.1. ■

APPENDIX B
PROOF OF THEOREM V.1

Here we prove Theorem V.1. To do so, we rely on Gronwall's inequality, which in general allows to bound the evolution of continuous-time and discrete-time signals described by differential and difference equations, respectively. Given the hybrid nature of the time-triggered dynamics (21), we rely on a version of Gronwall's inequality for hybrid systems developed in [24]. Adapted for our purposes, it states the following.

Proposition B.1. *(Generalized Gronwall's inequality [24]): Let $t \mapsto y(t) \in \mathbb{R}$ be a continuous signal, $t \mapsto p(t) \in \mathbb{R}$ be a continuously differentiable signal, $r := \{r_j\}_{j=0}^{k-1}$ be a nonnegative sequence of real numbers, $q \ge 0$ a constant, and $E := \{t_j\}_{j=0}^{k+1}$, $k \in \mathbb{Z}_{\ge 0}$ be a sequence of times satisfying $t_j < t_{j+1}$ for all $j \in \{0,\dots,k\}$. Suppose that for all $t \in [t_0, t_{k+1}]$, the elements y, p, and r satisfy*

$$y(t) \le p(t) + q\int_{t_0}^t y(s)ds + \sum_{j=0}^{i(t)-1} r_j y(t_{j+1})$$

with $i(t) := \max\{i \in \mathbb{Z}_{\ge 0} : t_i \le t, t_i \in E\}$ for $t < t_{k+1}$ and $i(t_{k+1}) := k$. Then,

$$y(t) \le p(t_0)h(t_0,t) + \int_{t_0}^t h(s,t)\dot{p}(s)ds$$

for all $t \in [t_0, t_{k+1}]$ where for all $t_0 \le s \le t \le t_{k+1}$,

$$h(s,t) := \exp\big(q(t-s) + \textstyle\sum_{j=i(s)}^{i(t)-1}\log(1+r_j)\big).$$

We are now ready to prove Theorem V.1.

Proof of Theorem V.1: Let $\{\{t_k^l\}_{k=0}^{N_l}\}_{l=0}^\infty$ be a sequence of times satisfying the hypotheses. Consider a trajectory $t \mapsto x(t)$ of (21) with $x(0)$ belonging to a neighborhood of $\bar{x}$. The definition of this neighborhood will show up later. Our proof strategy involves showing the monotonic decrease of the function W_ϵ (cf. (17)) along this arbitrarily chosen trajectory. Consider any $t \in \mathbb{R}_{\ge 0}$ such that $t \notin \{t_k^l\}_{k=0}^{N_l}$ for any $l \in \mathbb{Z}_{\ge 0}$ and $x(t) \in \Omega$ where Ω is defined by (18). With a slight abuse of notation let l and $k \in \{0,\dots,N_l - 1\}$ be fixed such that $t \in (t_k^l, t_{k+1}^l)$. Then, using the expression of $F(x) = f(x) + g(x) + h(x)$ given in (23), one can write the evolution of x at t for the considered trajectory as

$$\dot{x}(t) = F(x(t)) + g(x(t_k^l)) - g(x(t)) + h(x(t_0^l)) - h(x(t)).$$

(I) Dissipation inequality: Note that at t the evolution of W_ϵ is equal to the dot product between the gradient of W_ϵ and right-hand side of the above equation. Hence, we get

$$\begin{aligned} \dot{W}_\epsilon(x(t)) = \nabla W_\epsilon(x(t))^\top \Big(&F(x(t)) + g(x(t_k^l)) - g(x(t)) \\ &+ h(x(t_0^l)) - h(x(t))\Big). \end{aligned} \tag{35}$$

From (19b), we have $\nabla W_\epsilon(x(t))^\top F(x(t)) \le -\alpha\|x(t)-\bar{x}\|^2$. Moreover, since maps ∇W_ϵ, g, and h are globally Lipschitz and $\nabla W_\epsilon(\bar{x}) = 0$, one has $\|\nabla W_\epsilon(x(t))\| \le L_W\|x(t)-\bar{x}\|$, $\|g(x(t_k^l)) - g(x(t))\| \le L_g\|x(t_k^l) - x(t)\|$, and $\|h(x(t_0^l)) - h(x(t))\| \le L_h\|x(t_0^l) - x(t)\|$. Using these bounds in (35), we get

$$\begin{aligned} \dot{W}_\epsilon(x(t)) \le -\alpha\|x(t)-\bar{x}\|^2 + L_W\|x(t)-\bar{x}\|\Big(&L_g\|x(t) \\ &- x(t_k^l)\| + L_h\|x(t) - x(t_0^l)\|\Big). \end{aligned} \tag{36}$$

Next, we provide bounds on $\|x(t) - x(t_k^l)\|$ and $\|x(t) - x(t_0^l)\|$ in terms of $\|x(t) - \bar{x}\|$, $t - t_k^l$, and $t - t_0^l$. To reduce the notational burden, we drop the superscript l from the time instances $\{t_i^l\}_{i=1}^{N_l}$. In addition, we define

$$\begin{aligned} &x_k := x(t_k), && \zeta_k(t) := t - t_k, \\ &\zeta_j^k := \zeta_j(t_k) = t_k - t_j, && \xi^l(t) := \zeta_0(t) = t - t_0. \end{aligned}$$

(II) Bounds on $\|\mathbf{x(t)} - \mathbf{x(t_k^l)}\|$: Note that $x(t)$ can be written using (22) as the line integral

$$\begin{aligned} x(t)-x_k &= \textstyle\int_{t_k}^t f(x(s))ds + \zeta_k(t)g(x_k) + \zeta_k(t)h(x_0) \\ &= \textstyle\int_{t_k}^t (f(x(s)) - f(x_k))ds + \zeta_k(t)(f(x_k) - f(\bar{x})) \\ &\quad + \zeta_k(t)(g(x_k) - g(\bar{x}) + h(x_0) - h(\bar{x})). \end{aligned} \tag{37}$$

Above, we have added and subtracted $\zeta_k(t)f(x_k)$ and subtracted $f(\bar{x}) + g(\bar{x}) + h(\bar{x})$ as $\bar{x}$ is an equilibrium. Using Lipschitz bounds and triangle inequality in (37) we obtain

$$\begin{aligned} \|x(t) - x_k\| &\leq L_f \textstyle\int_{t_k}^t \|x(s) - x_k\|ds \\ &\quad + \zeta_k(t)(L_f + L_g)\|x_k - \bar{x}\| + \zeta_k(t)L_h\|x_0 - \bar{x}\|. \end{aligned} \tag{38}$$

From above, we wish to obtain an upper bound on $\|x(t)-x_k\|$ that is independent of the state at times $s \in (t_k, t)$. To this end, we employ Gronwall's inequality as stated in a general form in Proposition B.1. Drawing a parallelism between the notations, for (38), we consider $E = \emptyset$, $r = 0, y(t) = \|x(t) - x_k\|, q = L_f, p(t) = \zeta_k(t)(L_f + L_g)\|x_k - \bar{x}\| + \zeta_k(t)L_h\|x_0 - \bar{x}\|$. Then, applying Proposition B.1 and integrating the then obtained right-hand side yields

$$\begin{aligned} \|x(t) - x_k\| &\leq \left(1 + \tfrac{L_g}{L_f}\right)\|x_k - \bar{x}\|(e^{L_f\zeta_k(t)} - 1) \\ &\quad + \tfrac{L_h}{L_f}\|x_0 - \bar{x}\|(e^{L_f\zeta_k(t)} - 1). \end{aligned} \tag{39}$$

Bounding the above inequality using the triangle inequality $\|x_k - \bar{x}\| \leq \|x(t) - x_k\| + \|x(t) - \bar{x}\|$, collecting coefficients of $\|x(t) - x_k\|$ on the left-hand side, and rearranging gives

$$\begin{aligned} \|x(t) - x_k\| &\leq \frac{L_h(e^{L_f\zeta_k(t)} - 1)}{L_f - (L_f + L_g)(e^{L_f\zeta_k(t)} - 1)}\|x_0 - \bar{x}\| \\ &\quad + \frac{(L_f + L_g)(e^{L_f\zeta_k(t)} - 1)}{L_f - (L_f + L_g)(e^{L_f\zeta_k(t)} - 1)}\|x(t) - \bar{x}\|. \end{aligned} \tag{40}$$

(III) Bounds on $\|\mathbf{x(t)} - \mathbf{x(t_0^l)}\|$: Our next step is to provide an upper bound on the term $\|x(t) - x_0\|$. Recall that the considered trajectory satisfies (22) and so, the line integral over the interval $[t_0, t]$ gives

$$\begin{aligned} x(t) - x_0 &= \textstyle\int_{t_0}^t f(x(s))ds + \sum_{j=0}^{k-1} \zeta_j^{j+1} g(x_j) \\ &\quad + \zeta_k(t)g(x_k) + \xi^l(t)h(x_0). \end{aligned}$$

As done before, on the right-hand side, we add and subtract the terms $\xi^l(t)f(x_0)$ and $\xi^l(t)g(x_0)$ and then subtract $f(\bar{x}) + g(\bar{x}) + h(\bar{x})$. This gives us

$$\begin{aligned} x(t) - x_0 &= \textstyle\int_{t_0}^t (f(x(s)) - f(x_0))ds \\ &\quad + \textstyle\sum_{j=0}^{k-1} \zeta_j^{j+1}(g(x_j) - g(x_0)) + \zeta_k(t)(g(x_k) - g(x_0)) \\ &\quad + \xi^l(t)(f(x_0) - f(\bar{x}) + g(x_0) - g(\bar{x}) + h(x_0) - h(\bar{x})) \end{aligned}$$

By defining $L := L_f + L_g + L_h$, taking the norms, using the global Lipschitzness, we obtain from above

$$\begin{aligned} \|x(t) - x_0\| &\leq L_f \textstyle\int_{t_0}^t \|x(s) - x_0\|ds + \xi^l(t)L\|x_0 - \bar{x}\| \\ &\quad + L_g \textstyle\sum_{j=0}^{k-1} \zeta_j^{j+1}\|x_j - x_0\| + L_g\zeta_k(t)\|x_k - x_0\|. \end{aligned}$$

Consider any $\hat{t} \in [t, t_{k+1}]$ and note that $\zeta_k(t) \leq \zeta_k(\hat{t})$. Using this bound and the fact that the first term in the above summation is zero, we write

$$\begin{aligned} \|x(t)-x_0\| &\leq L_f \textstyle\int_{t_0}^t \|x(s) - x_0\|ds + \xi^l(t)L\|x_0 - \bar{x}\| \\ &\quad + L_g \textstyle\sum_{j=0}^{k-2} \zeta_{j+1}^{j+2}\|x_{j+1} - x_0\| + L_g\zeta_k(\hat{t})\|x_k - x_0\|. \end{aligned}$$

We now apply Proposition B.1 to give a bound for the left-hand side independent of $x(s)$, $s \in (t_0, t]$. In order to do so, the elements corresponding to those in the Gronwall's inequality are: $E = \{t_j\}_{j=0}^k \cup \{\hat{t}\}$, $y(t) = \|x(t) - x_0\|, p(t) = \xi^l(t)L\|x_0 - \bar{x}\|, q = L_f, r_j = L_g\zeta_{j+1}^{j+2}$ for $j = 0, \ldots, k-2$, and $r_{k-1} = \hat{t} - t_k$. From Proposition B.1, we get

$$\|x(t) - x_0\| \leq L\|x_0 - \bar{x}\| \textstyle\int_{t_0}^t h(s,t)ds, \tag{41}$$

where $h(s,t) = \exp\big(\int_s^t L_f dT + \sum_{j=i(s)}^{k-2} \log(1 + \zeta_{j+1}^{j+2}L_g) + \log(1 + L_g\zeta_k(\hat{t}))\big)$ and $i(s)$ is as defined in Proposition B.1. Using $\log(1 + x) \leq x$ for $x \geq 0$ and the fact that the exponential is a monotonically increasing function, we get

$$h(s,t) \leq \exp\left(L_f(t - s) + L_g \textstyle\sum_{j=i(s)}^{k-2} \zeta_{j+1}^{j+1} + L_g\zeta_k(\hat{t})\right).$$

By noting that $s \leq i(s) + 1$ and $t \leq \hat{t}$, we can upper bound the right-hand side as $h(s,t) \leq \exp\big(L_f(t - s) + L_g(\hat{t} - s)\big)$. Since $\hat{t}$ was chosen arbitrarily in the interval $[t, t_{k+1}]$, we pick it equal to t. Thus, $h(s,t) \leq \exp\left((L_g + L_f)(t - s)\right)$. Substituting this inequality in (41) yields

$$\begin{aligned} \|x(t) - x_0\| &\leq L\|x_0 - \bar{x}\| \textstyle\int_{t_0}^t e^{(L_f+L_g)(t-s)}ds \\ &= \tfrac{L}{L_f+L_g}(e^{(L_f+L_g)\xi^l(t)} - 1)\|x_0 - \bar{x}\|. \end{aligned} \tag{42}$$

This inequality when used in the right-hand side of the triangle inequality $\|x_0 - \bar{x}\| \leq \|x(t) - x_0\| + \|x(t) - \bar{x}\|$ yields after rearrangement the following

$$\|x_0 - \bar{x}\| \leq \frac{L_f + L_g}{L_f + L_g - L(e^{(L_f+L_g)\xi^l(t)} - 1)}\|x(t) - \bar{x}\|. \tag{43}$$

Subsequently, using the above bound in (42) gives

$$\|x(t) - x_0\| \leq \frac{L(e^{(L_f+L_g)\xi^l(t)} - 1)}{L_f + L_g - L(e^{(L_f+L_g)\xi^l(t)} - 1)}\|x(t) - \bar{x}\|. \tag{44}$$

Combining inequalities (40) and (43) we obtain

$$\begin{aligned} \|x(t) - x_k\| &\leq \frac{L_h(e^{L_f\zeta_k(t)} - 1)}{L_f - (L_f + L_g)(e^{L_f\zeta_k(t)} - 1)} \cdot \\ &\quad \frac{L_f + L_g}{L_f + L_g - L(e^{(L_f+L_g)\xi^l(t)} - 1)}\|x(t) - \bar{x}\| \\ &\quad + \frac{(L_f + L_g)(e^{L_f\zeta_k(t)} - 1)}{L_f - (L_f + L_g)(e^{L_f\zeta_k(t)} - 1)}\|x(t) - \bar{x}\| \end{aligned} \tag{45}$$

(IV) Monotonic decrease of $\mathbf{W_\epsilon}$: Note first that following (44) and using the bound $\xi^l(t) \leq \bar{\xi}$ yields

$$\|x(t) - x_0\| \leq \frac{L(e^{(L_f+L_g)\bar{\xi}} - 1)}{L_f + L_g - L(e^{(L_f+L_g)\bar{\xi}} - 1)}\|x(t) - \bar{x}\|.$$

Using the definition of $\bar{\xi}$, one gets $e^{(L_f+L_g)\bar{\xi}} - 1 = \frac{\beta(L_f+L_g)}{L(L_W L_h+\beta)}$. Substituting this value in the above inequality and simplifying the expression provides us

$$\|x(t) - x_0\| \leq (\beta/(L_W L_h))\|x(t) - \bar{x}\|. \tag{46}$$

In a similar way, using the bound on $\xi^l(t)$ and substituting the value of $e^{(L_f+L_g)\bar{\xi}}-1$ in (45) and simplifying yields

$$\|x(t)-x_k\| \leq \frac{(e^{L_f\zeta_k(t)}-1)(L+\beta/L_W)}{L_f-(L_f+L_g)(e^{L_f\zeta_k(t)}-1)}\|x(t)-\bar{x}\|.$$

Note that $\zeta_k(t) \leq \bar{\zeta}$. Using this bound and the definition of $\bar{\zeta}$ in the above inequality gives

$$\|x(t)-x_k\| \leq \tfrac{\alpha-\beta}{L_W L_g}\|x(t)-\bar{x}\|. \tag{47}$$

Finally, substituting (46) and (47) in (36) and using the fact that $\beta < \alpha$, we obtain $\dot{W}_\epsilon(x(t)) < 0$. Recall that $t \in \mathbb{R}_{\geq 0}$ was chosen arbitrarily satisfying $t \notin \{t_k^l\}_{k=1}^{N_l}$ for any $l \in \mathbb{Z}_{\geq 0}$. Therefore, W_ϵ monotonically decreases at all times along the trajectory except for a countable number of points. Further, the map $t \mapsto W_\epsilon(x(t))$ is continuous. Therefore, we conclude that the trajectory initialized in a compact level set of W_ϵ contained in Ω converges asymptotically to the equilibrium point $\bar{x}$. This completes the proof. ■

REFERENCES

[1] T. W. Stegink, A. Cherukuri, C. De Persis, A. J. van der Schaft, and J. Cortés, "Integrating iterative bidding in electricity markets and frequency regulation," in *American Control Conference*, Milwaukee, Wisconsin, USA, 2018, to appear.

[2] F. Dörfler, J. W. Simpson-Porco, and F. Bullo, "Breaking the hierarchy: Distributed control and economic optimality in microgrids," *IEEE Transactions on Control of Network Systems*, vol. 3, no. 3, pp. 241–253, 2016.

[3] X. Zhang and A. Papachristodoulou, "A real-time control framework for smart power networks: Design methodology and stability," *Automatica*, vol. 58, pp. 43–50, 2015.

[4] S. Trip, M. Bürger, and C. De Persis, "An internal model approach to (optimal) frequency regulation in power grids with time-varying voltages," *Automatica*, vol. 64, pp. 240–253, 2016.

[5] S. T. Cady, A. D. Domínguez-García, and C. N. Hadjicostis, "A distributed generation control architecture for islanded AC microgrids," *IEEE Transactions on Control Systems Technology*, vol. 23, no. 5, pp. 1717–1735, 2015.

[6] N. Li, C. Zhao, and L. Chen, "Connecting automatic generation control and economic dispatch from an optimization view," *IEEE Transactions on Control of Network Systems*, vol. 3, no. 3, pp. 254–264, 2016.

[7] Y. Zhang, M. Hong, E. Dall'Anese, S. Dhople, and Z. Xu, "Distributed controllers seeking AC optimal power flow solutions using ADMM," *IEEE Transactions on Smart Grid*, 2018, to appear.

[8] E. Dall'Anese, S. V. Dhople, and G. B. Giannakis, "Photovoltaic inverter controllers seeking ac optimal power flow solutions," *IEEE Transactions on Power Systems*, vol. 31, no. 4, pp. 2809–2823, 2016.

[9] F. Alvarado, J. Meng, C. DeMarco, and W. Mota, "Stability analysis of interconnected power systems coupled with market dynamics," *IEEE Transactions on Power Systems*, vol. 16, no. 4, pp. 695–701, 2001.

[10] D. J. Shiltz, M. Cvetković, and A. M. Annaswamy, "An integrated dynamic market mechanism for real-time markets and frequency regulation," *IEEE Transactions on Sustainable Energy*, vol. 7, no. 2, pp. 875–885, 2016.

[11] D. J. Shiltz, S. Baros, M. Cvetković, and A. M. Annaswamy, "Integration of automatic generation control and demand response via a dynamic regulation market mechanism," *IEEE Transactions on Control Systems Technology*, 2018, to appear.

[12] T. Stegink, C. De Persis, and A. van der Schaft, "A unifying energy-based approach to stability of power grids with market dynamics," *IEEE Transactions on Automatic Control*, vol. 62, no. 6, pp. 2612–2622, 2017.

[13] A. Cherukuri and J. Cortés, "Iterative bidding in electricity markets: rationality and robustness," *arXiv preprint arXiv:1702.06505*, 2017, submitted to *IEEE Transactions on Control of Network Systems*.

[14] T. W. Stegink, A. Cherukuri, C. De Persis, A. J. van der Schaft, and J. Cortés, "Frequency-driven market mechanisms for optimal dispatch in power networks," in *IEEE Transactions on Automatic Control*, 2017, submitted.

[15] J. Machowski, J. Bialek, and J. Bumby, *Power System Dynamics: Stability and Control*, 2nd ed. Ltd: John Wiley & Sons, 2008.

[16] F. Dörfler and F. Bullo, "Synchronization in complex networks of phase oscillators: A survey," *Automatica*, vol. 50, no. 6, pp. 1539–1564, 2014.

[17] A. Cherukuri and J. Cortés, "Decentralized Nash equilibrium learning by strategic generators for economic dispatch," in *American Control Conference*. IEEE, 2016, pp. 1082–1087.

[18] D. Fudenberg and J. Tirole, *Game Theory*. Cambridge, MA: MIT Press, 1991.

[19] S. Stoft, "Power system economics," *Journal of Energy Literature*, vol. 8, pp. 94–99, 2002.

[20] S. Boyd, N. Parikh, E. Chu, B. Peleato, and J. Eckstein, "Distributed optimization and statistical learning via the alternating direction method of multipliers," *Foundations and Trends in Machine Learning*, vol. 3, no. 1, pp. 1–122, 2011.

[21] E. D. Sontag and Y. Wang, "New characterizations of input-to-state stability," *IEEE Transactions on Automatic Control*, vol. 41, no. 9, pp. 1283–1294, 1996.

[22] H. K. Khalil, *Nonlinear systems*. Prentice Hall, New Jersey, 1996, vol. 3.

[23] J. Cortés, "Discontinuous dynamical systems - a tutorial on solutions, nonsmooth analysis, and stability," *IEEE Control Systems Magazine*, vol. 28, no. 3, pp. 36–73, 2008.

[24] N. Noroozi, D. Nešić, and A. R. Teel, "Gronwall inequality for hybrid systems," *Automatica*, vol. 50, no. 10, pp. 2718–2722, 2014.